採取した。培養液中に注射器で骨髄細胞を洗い出す。ナイロンメッシュを通した後、遠心、洗浄を繰り返し、骨髄細胞調製液を得た。実験により成熟T細胞は抗マウスCD90(Thy-1.2抗体)と磁気ビーズを用いて除去した。

骨髄移植を受けるレシピエントマウスには、15-30週齢のDMRVおよび同腹仔を用いた。マウスには、移植1週間前から移植後2週間までアンピシリン水を与えた。　放射線照射は日立X線照射装置MBR-1520R-3を用いて、9-12GreyのX線(12Greyの場合は6Greyずつ2分割)を照射した。骨髄移植は、1-2X10^6(500μl培地)の骨髄細胞を尾静脈より注射した。

血液細胞のキメラ率の測定は、ヘパリン採血した末梢血から赤血球を溶解したのち、白血球のみを蛍光顕微鏡下にカウントした。シアル酸の定量は、シアル酸を蛍光誘導体化して、HPLCにて定量化した。

(倫理面への配慮)

すべての動物実験は、国立精神・神経センター神経研究所動物実験に関する倫理指針に従い行い、同研究所小型実験動物倫理問題検討委員会にて審査・承認を得ている。すべての組み換えDNA実験は、カルタヘナ議定書に基づく「遺伝子組み換え生物等の使用等の規制による生物の多様性の確保に関する法律」と関係省令を遵守し、国立精神・神経センター神経研究所組み換えDNA実験安全委員会の審査・承認を得て行なっている。

C. 研究結果

一匹のGFP-Tgマウスから単離した骨髄細胞液中の細胞数は約3 x 10^6 であり、CD90抗体により、60%が素通り画分に、40%が磁気ビーズ吸着画分に回収された。各画分に回収された細胞の染色では、素通り画分にはCD90陽性細胞は含まれていなかった。

12Greyの放射線を与えられたマウスに、未精製骨髄細胞を移植した。遺伝子型に関わらず、移植後1週間で約90%のマウスが死亡した。また、生き残った個体にも、背側全体に白髪化と皮膚障害が見られた。そこで、9Greyの放射線照射と成熟T細胞を除去した骨髄細胞を移植することに条件を変えた。9Greyの照射では、移植後1週間で約10%のマウスのみが死亡したが、生存マウスには際立った外観的な異常は見られなかった。

末梢血の白血球のキメラ率は、約70-85%のGFP陽性率であり、ほとんどがドナー由来の骨髄細胞で占められていたが、移植後の時間経過とともに若干低下傾向にあった。血清シアル酸レベルの測定では、最もシアル酸量が増加したマウスでは、移植後11週で0.181nmol/lであり、昨年度シアル酸を投与したマウスに比べ、高値を示した。

D. 考察

GFP-Tgマウスから骨髄細胞を調製し、DMRVマウスへの移植実験を行った。同時に条件最適化の検討を行なった。腸管への障害を防ぐため、比較的弱い放射線を二度に分けて照射する方法を試したが、ほとんどのマウスが一週間後、死に至ってしまった。死亡マウスは、死亡時に際立った特徴を示さなかったが、生存マウスは白髪化と皮膚障害という典型的な放射線障害像を示した。そこで、照射量を減少した単回照射に変更し、また、磁気ビーズ法により成熟T細胞を取り除いた後に骨髄細胞を移植する方法にした結果、マウスの生存率が格段に改善した。マウスの放射線に対する感受性はstrainによって異なり、129SVは比較的弱いという報告もある。現在、どの因子が重要であるのかを解析している。

骨髄移植によって血清のシアル酸含量は、DMRV非治療群に比べ、2倍以上増加した。今後は、移植白血球でのGNE活性の測定ともに、骨髄細胞のある幹細胞の各臓器への取り込みを調べる予定である。また、マウスの表現型の解析を開始していく予定である。

E. 結論

GFP-Tgマウスからの骨髄細胞をDMRVモデルマウスに移植した。移植マウスの血球のキメラ率は70-85%であり、血清のシアル酸は2倍以上の増加を示した。

F. 健康危険情報

特になし

G. 研究発表

1．論文発表

Ohkuma A, Nonaka I, Malicdan MCV, Noguchi S, Nomura K, Sugie H, Hayashi YK, Nishino I: Distal lipid storage myopathy due to PNPLA2 mutation. *Neuromuscul Disord* 18: 671-674, 2008

Malicdan MCV, Noguchi S, Hayashi YK, Nishino I: Muscle weakness correlates with muscle atrophy and precedes the development of inclusion body or rimmed vacuoles in the mouse model of DMRV/hIBM. *Physiol Genomics* 35: 106-115, 2008

Kawahara G, Ogawa M, Okada M, Malicdan MCV, Goto Y, Hayashi YK, Noguchi S, Nishino I: Diminished binding of mutated collagen VI to the extracellular matrix surrounding myocytes. *Muscle Nerve* 38: 1192-1195, 2008

Ohkuma A, Noguchi S, Sugie H, Malicdan MCV, Fukuda T, Shimazu K, López LC, Hirano M, Hayashi YK, Nonaka I, Nishino I. Clinical and genetic analysis of lipid storage myopathies. *Muscle Nerve* 39: 333-342, 2009

2．学会発表

門間一成, 野口　悟, 林由起子, 南　成祐, 元吉和夫, 鎌倉恵子, 埜中征哉, 西野一三：Becker型筋ジストロフィーにおける縁取り空胞の出現に関する臨床病理学的検討. 第49回日本神経学会総会,　横浜, 5.16, 2008

野口　悟, Malicdan MCV, 林由起子, 西野一三: 縁取り空胞を伴う遠鋳型ミオパチーモデルマウスの生理学的解析. 第31回日本分子生物学会 第81回日本生化学会合同大会, 神戸, 12.12, 2008

Malicdan MCV, Noguchi S, Hayashi YK, Nonaka I, Nishino I: Amyloidogenesis in a mouse model of DMRV/hIBM. Congress of the World Muscle Society (WMS), Newcastle Upon Tyne, United Kingdom, 9.30, 2008

Nishino I, Oya Y, Monma K, Noguchi S, Hayashi YK, Nonaka I: Cytoplasmic body with acid phosphatase activity-Hallmark of adult-onset Pompe disease on muscle pathology. Congress of the World Muscle Society (WMS), Newcastle Upon Tyne, United Kingdom, 10.1, 2008

Monma K, Noguchi S, Hayashi YK: Clinico-pathological characteristics of the Becker muscle dystrophy with rimmed vacuole. Congress of the World Muscle Society (WMS), Newcastle Upon Tyne, United Kingdom, 10.1, 2008

H. 知的財産権の出願・登録状況（予定を含む）

1．特許取得

特になし

2．実用新案登録

特になし

3．その他

特になし

Ⅲ.　研究成果の刊行に関する一覧表

研究成果の刊行に関する一覧表

発表者氏名： 論文タイトル名．発表誌名 巻号： ページ，出版年
Ohkuma A, Nonaka I, Malicdan MCV, Noguchi S, Nomura K, Sugie H, Hayashi YK, Nishino I: Distal lipid storage myopathy due to PNPLA2 mutation. *Neuromuscul Disord* 18: 671-674, 2008
Malicdan MCV, Noguchi S, Hayashi YK, Nishino I: Muscle weakness correlates with muscle atrophy and precedes the development of inclusion body or rimmed vacuoles in the mouse model of DMRV/hIBM. *Physiol Genomics* 35: 106-115, 2008
Kawahara G, Ogawa M, Okada M, Malicdan MCV, Goto Y, Hayashi YK, Noguchi S, Nishino I: Diminished binding of mutated collagen VI to the extracellular matrix surrounding myocytes. *Muscle Nerve* 38: 1192-1195, 2008
Malicdan MCV, Noguchi S, Nonaka I, Saftig P, Nishino I: Lysosomal myopathies: An excessive build-up in autophagosomes is too much to handle. *Neuromuscul Disord* 18: 521-529, 2008
Malicdan MCV, Noguchi S, Nishino I: Recent advances in distal myopathy with rimmed vacuoles (DMRV) or hIBM: treatment perspectives. *Curr Opin Neurol* 21: 596-600, 2008
Ohkuma A, Noguchi S, Sugie H, Malicdan MCV, Fukuda T, Shimazu K, López LC, Hirano M, Hayashi YK, Nonaka I, Nishino I. Clinical and genetic analysis of lipid storage myopathies. *Muscle Nerve* 39: 333-342, 2009

Ⅳ.　研究成果の刊行物・別刷

Neuromuscular Disorders 18 (2008) 671–674

www.elsevier.com/locate/nmd

Case report

Distal lipid storage myopathy due to *PNPLA2* mutation

Aya Ohkuma [a,b,c], Ikuya Nonaka [a], May Christine V. Malicdan [a], Satoru Noguchi [a], Satoru Ohji [b], Kyoichi Nomura [b], Hideo Sugie [d], Yukiko K. Hayashi [a], Ichizo Nishino [a,*]

[a] *Department of Neuromuscular Research, National Institute of Neuroscience, National Center of Neurology and Psychiatry (NCNP), 4-1-1 Ogawahigashi-cho, Kodaira, Tokyo 187-8502, Japan*

[b] *Department of Neurology, Saitama Medical Center, Saitama, Japan*

[c] *Department of Neurology, Saitama Medical University, Saitama, Japan*

[d] *Jichi Children's Medical Center Tochigi, Jichi Medical University, Tochigi, Japan*

Received 8 January 2008; received in revised form 22 June 2008; accepted 24 June 2008

Abstract

Distal myopathy is a group of heterogeneous disorders affecting predominantly distal muscles usually appearing from young to late adulthood with very rare cardiac complications. We report a 27-year-old man characterized clinically by distal myopathy and dilated cardiomyopathy, pathologically by lipid storage, and genetically by a *PNPLA2* mutation. The patient developed weakness in his lower legs and fingers at age 20 years. Physical examination at age 27 years revealed muscle weakness and atrophy predominantly in lower legs and hands, and severe dilated cardiomyopathy. The patient had a homozygous four-base duplication (c.475_478dupCTCC) in exon 4 of *PNPLA2*.

Keywords: Distal myopathy; Lipid storage myopathy; Neutral lipid storage disease with myopathy; *PNPLA2*

1. Introduction

Lipid storage myopathy (LSM) is a pathologically defined entity with accumulation of triglycerides in the muscle fiber. Six causative genes for only four diseases have been identified: *SLC22A5* for primary carnitine deficiency (PCD); *ETFA*, *ETFB*, and *ETFDH* for multiple acyl-CoA dehydrogenase deficiency (MADD); *ABHD5* for neutral lipid storage disease with ichthyosis or Chanarin–Dorfman syndrome; and *PNPLA2* for neutral lipid storage disease with myopathy (NLSDM) [1–3].

PNPLA2 encodes an adipose triglyceride lipase; mutations in this gene were recently reported in three patients who presented with LSM and variable cardiac involvement [1]. Here, we report a Japanese patient with a *PNPLA2* mutation presenting with distal myopathy and severe dilated cardiomyopathy and showing numerous rimmed vacuoles on muscle pathology.

2. Case report

A 27-year-old man had slowly progressive muscle weakness. Despite being a slow runner since childhood, he belonged to a mountaineering club and had no difficultly climbing mountains. At 20 years, he noticed difficulty climbing down the stairs, and gradually developed distal dominant muscle weakness and atrophy. Family history was non-contributory.

Upon consultation with us at 27 years, he had marked muscle weakness and atrophy in the extremities predominantly in the lower legs (Fig. 1A) and fingers (Fig. 1B). Examination of the muscle strength showed 3–4/5 asymmetric weakness over the deltoid, biceps brachii, extensor digitorum, gastrocnemius, and tibialis anterior. Grasping power was 12 kg on right and 10 kg on left (normal

* Corresponding author. Tel.: +81 42 346 1712; fax: +81 42 346 1742.
E-mail address: nishino@ncnp.go.jp (I. Nishino).

0960-8966/$ - see front matter © 2008 Elsevier B.V. All rights reserved.
doi:10.1016/j.nmd.2008.06.382

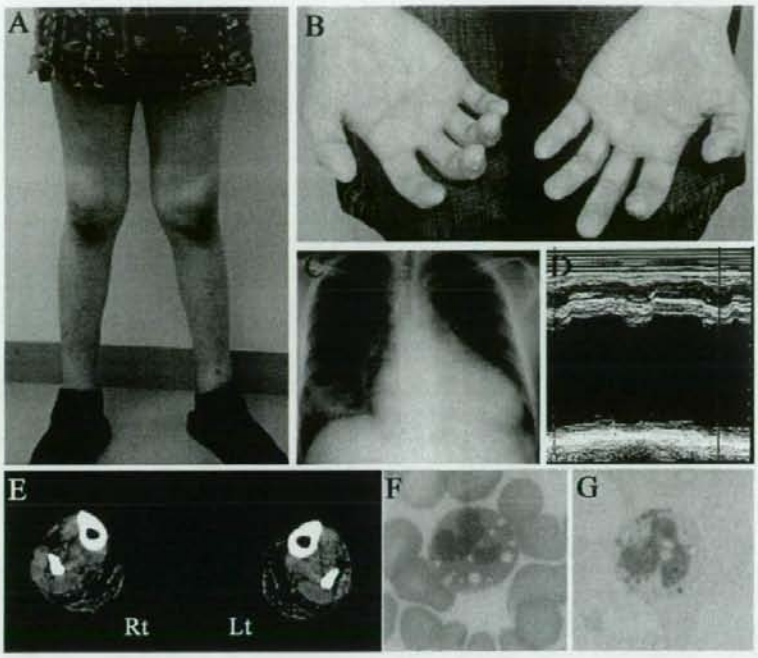

Fig. 1. The patient had distal muscle atrophy especially in the lower legs (A) and thenar muscles (B). Chest X-ray showed cardiomegaly with cardiothoratic ratio of 63% (normal cardiothoratic ratio <50%) (C). Echocardiogram showed left ventricular enlargement with decreased ejection fraction of 18% (normal >60%) (D). Calf muscles were involved relatively sparing tibialis anterior on CT (E). Note many vacuoles of leukocyte by Wright–Giemsa (F), which are positively stained by oil red O (G).

values = 43–56 kg). Deep tendon reflexes were absent. No skin abnormality was seen. Chest X-ray revealed cardiomegaly (Fig. 1C). Echocardiogram showed left ventricular enlargement with decreased left ventricular ejection fraction of 18% (normal >60%), left ventricular end-diastolic dimension of 78 mm, left ventricular end-systolic dimension of 70 mm, interventricular septum thickness of 8 mm and posterior wall thickness of 8 mm (Fig. 1D). ECG showed negative Q wave in lead I, negative P wave in V_1 and occasional ventricular extra-systoles. EMG showed myopathic changes. His respiratory function was normal. Serum creatine kinase was elevated (412–1697 IU/L; normal value <170). Serum cholesterol, TG, LDL-cholesterol and glucose were within normal ranges. In leukocytes, Jordans anomaly [4], multiple tiny vacuoles due to lipid accumulation, was seen (Fig. 1F and G). Muscle CT showed decreased densities in both soleus, both gastrocnemius, and right tibialis anterior muscles (Fig. 1E).

Muscle biopsy from the left biceps brachii muscle revealed marked variation in fiber size. Numerous lipid droplets were seen in virtually all type one fibers (Fig. 2A). In addition, rimmed vacuoles were observed in scattered fibers (Fig. 2B). Dystrophin, caveolin-3, and dysferlin immunohistochemistry were normal. On electron microscopy, markedly increased lipid droplets were seen between myofibrils where mitochondria appeared pyknotic (Fig. 3A). Numerous autophagic vacuoles were also observed (Fig. 3B). Total and free muscle carnitine levels were 13.2 and 3.9 nmol/mg non-collagen protein, respectively (reference: total, 15.7 ± 2.8; free, 12.9 ± 3.7).

We sequenced all exons and the flanking intronic regions of all six known causative genes for LSM in genomic DNA. In the patient, we identified a homozygous four-base duplication (c.475_478dupCTCC) in exon 4 of *PNPLA2* (Gene ID: 57104), predicted to result in a premature stop codon at amino acid position 178. Heterozygous c.475_478dupCTCC mutation was confirmed in both healthy parents. We did not find any sequence variant in other candidate genes, including *GNE* gene.

3. Discussion

The patient presented has been followed up with a tentative diagnosis of distal myopathy. In fact, one patient in the first report of *PNPLA2* mutations had distal dominant muscle weakness although the other two had proximal muscle involvement [1]. Therefore, distal myopathy may not be uncommon in LSM associated with *PNPLA2* mutations.

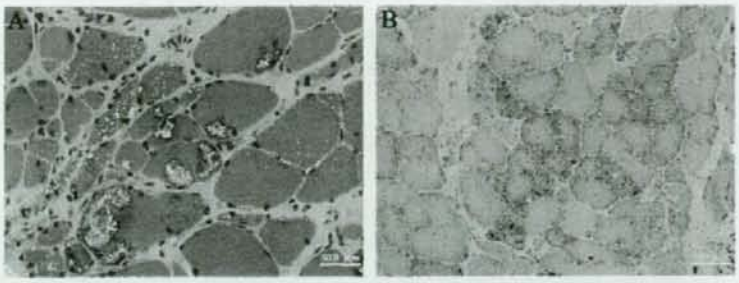

Fig. 2. In addition to variation in fiber size, numerous small vacuoles and rimmed vacuoles were seen with H&E staining (A). Numerous lipid droplets were seen with oil red O (B).

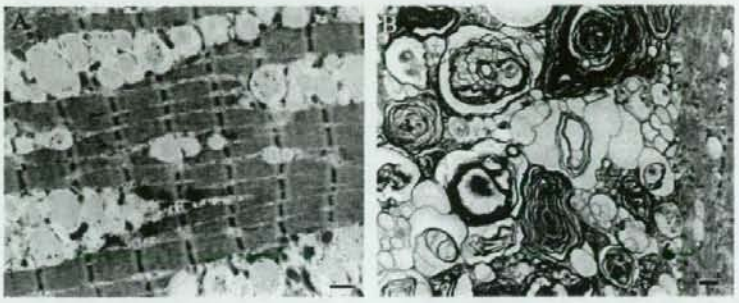

Fig. 3. Onelectron microscopy, markedly increased lipid droplets were seen intermyofibrillar spaces in most of fibers (A). In areas with the rimmed vacuoles, the lipid droplets were not actively scavenged by autophagosome (K). Bar = 1 μm.

Miyoshi myopathy and distal myopathy with rimmed vacuoles are the two most common distal myopathies in Japan, but these were excluded by immunohistochemistry for dysferlin and sequence analysis of *GNE* gene; moreover, finger muscle atrophy and weakness are not usually seen in these distal myopathies. There is a peculiar distal myopathy due to caveolin-3 gene mutation that selectively affected small muscles in hands and feet [5]. However, caveolin-3 immunohistochemistry was normal (data not shown).

Rimmed vacuoles can also be seen in myofibrillar myopathy and inclusion body myopathy with Paget's disease of bone and frontotemporal dementia (IBMPFD) [6,7]. Myofibrillar myopathy is pathologically characterized by disorganization of myofibrillar alignment and protein aggregations, such as cytoplasmic body and spheroid body, which were absent in our patient. IBMPFD is caused by mutations in the gene encoding valosin-containing protein and is clinically characterized by variable extent of dementia and polyostotic skeletal disorganization. IBMPFD is unlikely as our patient had neither intellectual deficit nor bone abnormality although Kimonis et al. recently postulated that IBMPFD is underdiagnosed and reported that 86% of patients had muscle disease while frontotemporal dementia and Paget disease of bone was diagnosed in 27% and 57%, respectively [8]. On top of it, lipid droplets are not a feature of any of the above-mentioned disorders.

In our patient, free carnitine was low in the muscle while total amount was normal. Two patients in the first report of *PNPLA2* mutations showed normal serum carnitine levels [1]. However, muscle carnitine levels were not measured in these patients. Further studies are necessary to determine a relationship between NLSDM and carnitine levels.

The increased amount of lipid droplets in muscle fibers led us to make a diagnosis of LSM. In PCD and MADD, lipid droplets are seen next to mitochondria that are structurally normal. In contrast, mitochondria are pyknotic in our case. Furthermore, autophagic vacuoles have never been reported in other LSM. These observations suggest a possibility that NLSDM may have a myodegenerative process different from other LSM.

We have 47 muscle biopsies diagnosed as LSM collected from 1978–2006. Interestingly, all other 46 patients had proximal dominant muscle weakness except for the present case, suggesting a possibility that distal muscle involvement may be unique to *PNPLA2* mutations although further studies are necessary to draw any conclusion.

Acknowledgement

This study is supported by the "Research on Psychiatric and Neurological Diseases and Mental Health" from Health and Labour Sciences Research Grants; the "Research on Health Sciences focusing on Drug Innovation"

from the Japanese Health Sciences Foundation; the "Research Grant (2OB-12, 2OB-13, 19A-4, and 19A-7) for Nervous and Mental Disorders" from the Ministry of Health, Labour and Welfare; the Program for Promotion of Fundamental Studies in Health Sciences of the National Institute of Biomedical Innovation (NIBIO).

References

[1] Fischer J, Lefevre C, Morava E, et al. The gene encoding adipose triglyceride lipase (PNPLA2) is mutated in neutral lipid storage disease with myopathy. Nat Genet 2007;39:28–30.

[2] Vockleya J, Whiteman D. Defects of mitochondrial beta-oxidation: growing group of disorders. Neuromuscul Disord 2002;12:235–46.

[3] Lefevre C, Jobard F, Caux F, et al. Mutations in CGI-58, the gene encoding a new protein of the esterase/lipase/thioesterase subfamily, in Chanarin–Dorfman syndrome. Am J Hum Genet 2001;69:1002–12.

[4] Jordan GH. The familial occurrence of fat containing vacuoles in the luekocytes diagnosed in two brothers suffering from dystrophica musculorum progressiva. Acta Med Scand 1953;145:419.

[5] Tateyama M, Aoki M, Nishino I, et al. Mutation in the caveolin-3 gene causes a peculiar form of distal myopathy. Neurology 2002;58:323–5.

[6] Kley RA, Hellenbroich Y, van der Ven PF, et al. Clinical and morphological phenotype of the filamin myopathy: a study of 31 German patients. Brain 2007;130:3250–64.

[7] Watts GD, Thomasova D, Ramdeen SK, et al. Novel VCP mutations in inclusion body myopathy associated with Paget disease of bone and frontotemporal dementia. Clin Genet 2007;72:420–6.

[8] Kimonis VE, Mehta SG, Fulchiero EC, et al. Clinical studies in familial VCP myopathy associated with Paget disease of bone and frontotemporal dementia. Am J Med Genet 2008;146A: 745–57.

Physiol Genomics 35: 106–115, 2008.
First published July 15, 2008; doi:10.1152/physiolgenomics.90219.2008.

Muscle weakness correlates with muscle atrophy and precedes the development of inclusion body or rimmed vacuoles in the mouse model of DMRV/hIBM

May Christine V. Malicdan, Satoru Noguchi, Yukiko K. Hayashi, and Ichizo Nishino

Department of Neuromuscular Research and Neuromuscular Research, National Institute of Neuroscience, National Center of Neurology and Psychiatry, Kodaira, Tokyo, Japan

Submitted 12 April 2008; accepted in final form 7 July 2008

Malicdan MC, Noguchi S, Hayashi YK, Nishino I. Muscle weakness correlates with muscle atrophy and precedes the development of inclusion body or rimmed vacuoles in the mouse model of DMRV/hIBM. *Physiol Genomics* 35: 106–115, 2008. First published July 15, 2008; doi:10.1152/physiolgenomics.90219.2008.—Distal myopathy with rimmed vacuoles (DMRV), also called hereditary inclusion body myopathy (hIBM), is characterized clinically by weakness and atrophy that initially involves the distal muscles and pathologically by the presence of rimmed vacuoles (RVs) or intracellular protein deposits in myofibers. It is caused by mutations in the UDP-*N*-acetylglucosamine 2-epimerase/*N*-acetylmannosamine kinase (*GNE*) gene that is important in sialic acid synthesis. Recently, we generated a mouse model (*Gne*$^{-/-}$ h*GNE*D176VTg) that exhibits muscle weakness and pathological changes similar to DMRV patients. To gain better understanding of the pathomechanism of DMRV, we determined temporal changes in the overall motor performance of this model mouse for DMRV in correlation with the structure and function of isolated skeletal muscles and muscle pathology. These DMRV mice exhibited muscle weakness, decreased whole muscle mass and cross-sectional area (CSA), and reduced contractile power in an age-related manner. Single-fiber CSA further supported the finding of muscle atrophy that involved both type I and type II fibers. These results suggest that atrophy is highly correlated with reduced production of force at young age, both in vivo and ex vivo, thereby implicating the important role of atrophy in the pathomechanism of DMRV. In older age, and particularly in gastrocnemius muscles, RVs and intracellular inclusions were seen in type IIA fibers, further aggravating reduction of force and specific increase in twitch-tetanus ratio.

distal myopathy with rimmed vacuoles/hereditary inclusion body myopathy; skeletal muscle force; amyloid

DISTAL MYOPATHY with rimmed vacuoles (DMRV) or hereditary inclusion body myopathy (hIBM) is an autosomal recessive disorder caused by mutations in the UDP-*N*-acetylglucosamine 2-epimerase/*N*-acetylmannosamine kinase (*GNE*) gene (9, 12, 21). This gene encodes the bifunctional enzyme catalyzing the two critical steps in sialic acid synthesis.

Because DMRV and hIBM are the same disorder, these terms are used synonymously here. DMRV predominantly affects distal muscles at the initial stages but also involves proximal muscles during the progression of the disease. This condition has been reported as quadriceps-sparing myopathy because the quadriceps muscles are relatively spared during the early stages of the disease (3). The skeletal muscles are primarily affected, but other organs, including cardiac muscles, were affected in a group of patients as well (20). The term used in the nosology of this condition partly arises from observations in pathological studies. In skeletal muscles, rimmed vacuoles (RVs) are seen in some fibers, in addition to the finding of scattered atrophic fibers and intracellular congophilic deposits that are immunoreactive to amyloid and tau, among other various proteins. Endomysial fibrosis, necrotic and regenerating process, and inflammatory cell infiltrates are not commonly seen but have been demonstrated in anecdotal reports. Although speculations and hypotheses abound regarding the pathomechanism to explain how these RVs are formed and how they could lead to muscle weakness (1, 2, 18, 22, 23, 25, 31, 32), precise information is not fully elucidated at this time.

Muscle weakness in DMRV has been attributed to several events. RV formation was generally believed to trigger a downstream cascade that ultimately leads to muscle fiber degeneration and atrophy. Deposition of inclusion bodies within myofibrils could physically interfere with the contractile apparatus, or could instigate a process of myofiber degeneration. RV formation in skeletal muscles, which indicates impaired autophagic process (15, 20, 23), is associated with reduced clearance of cytosolic proteins through basal autophagy; the resulting accumulation of autophagic vacuoles may interfere with the function of skeletal muscle. The contribution of each phenomenon to muscle weakness and how these events relate to each other have not been fully verified primarily because of the lack of a detailed time-course study, which is rather difficult to accomplish in patients with gradually progressive illnesses.

We recently generated the first mouse model for this myopathy that resembles the phenotype in humans (16). *Gne*$^{-/-}$ h*GNE*D176VL-Tg mice, which we refer to here as "DMRV mice," exhibited hyposialylation of serum and various organs, muscle weakness, and mild to moderate serum creatine kinase elevation from 30 wk of age, a time during which only subtle changes were seen in skeletal and cardiac muscles in addition to intracellular deposition of amyloid β in a few fibers. From 40 wk onward, RVs were seen in scattered fibers (15).

The primary pathogenesis in most murine models for muscular dystrophy can be traced to a common defect on the dystrophin-glycoprotein complex (DGC) that initiates a sequence of events that eventually lead to necrosis or apoptosis partly due to increased intracellular calcium (14). In DMRV

Address for reprint requests and other correspondence: S. Noguchi, Dept. of Neuromuscular Research and Neuromuscular Research, National Inst. of Neuroscience, National Ctr. of Neurology and Psychiatry, Kodaira, Tokyo, Japan (e-mail: noguchi@ncnp.go.jp).

The costs of publication of this article were defrayed in part by the payment of page charges. The article must therefore be hereby marked "*advertisement*" in accordance with 18 U.S.C. Section 1734 solely to indicate this fact.

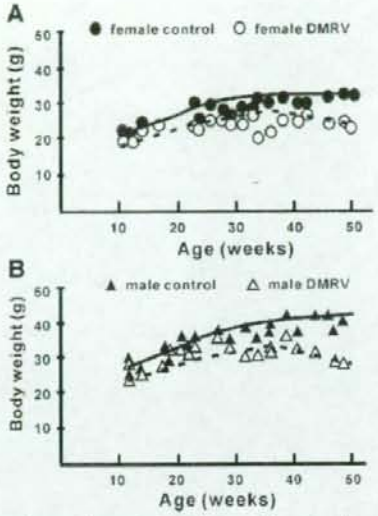

Fig. 1. General morphology of mice. *A*: body weight of female mice. *B*: body weight of male mice. Distal myopathy with rimmed vacuoles (DMRV) mice were at least 5–10% smaller at 10 wk of age and only showed small increases of body mass with age; hence from the age of 31 wk they are 20–30% smaller than their age-matched control littermates.

mice, however, we have excluded at least the "leaky hypothesis," because they have intact DGC complex, and this is supported by the paucity of necrotic and regenerating process. The absence of definite sarcolemmal defect, nevertheless, is also seen in other murine models of muscular dystrophies (8, 11, 26), making the origin of loss of force generation in these murine models far from being understood. Unfortunately, very few studies have addressed the mechanism of muscle weakness in nondystrophic states, including chronic myopathies.

Our previous results prompted us to work on several hypotheses. First, we hypothesize that factors other than the presence of pathological hallmarks play an important role in the pathogenesis of muscle weakness, because we have seen generalized body weakness at the age when there were no obvious pathological findings. Second, we think that the mechanism underlying muscle weakness is distinct from the theories established in other muscular dystrophies. Finally, because some muscles are relatively spared from the formation of RVs and intracellular inclusion, the degree of effect is most likely not the same among different muscles. Thus a study focusing on the structure and function of the muscles of these DMRV mice is appropriate, and could help us discover further clues that we could use in developing methods useful for evaluating treatment strategies for this debilitating myopathy.

METHODS

Ethical approval. All animal experiments conducted in this study were approved by and carried out in accordance with the rules and regulations of the Ethical Review Committee on the Care and Use of Rodents in the National Institute for Neuroscience, National Center of Neurology and Psychiatry (NCNP). These policies are based on the "Guidelines for Animal Experimentation," as sanctioned by the Council of the Japanese Association of Laboratory Animal Science.

Animal groups. Generation of *Gne*-knockout mice that express the human *GNE* mutation D176V was described previously (16). In the present study, we used the same line of *Gne*$^{-/-}$ hGNED176VL-Tg mice (DMRV mice). Four groups of DMRV mice were studied: 10–20 wk, 21–30 wk, 31–40 wk, and 41–50 wk of age; each group consisted of five males and five females. Age-matched and sex-matched littermates (*Gne*$^{+/+}$ or *Gne*$^{-/-}$hGNED176VL-Tg) served as controls. All animals were housed in a barrier-protected facility that strictly adhered to specific pathogen-free-grade maintenance at the National Institute of Neurosciences, NCNP. The animals were maintained on a 12:12-h light-dark cycle and given unlimited access to food and water.

Treadmill exercise tests. Mice were exercised on a 10-lane treadmill (MK-680, Muromachi, Tokyo, Japan) with an adjustable belt speed and equipped with adjustable-amperage shock bars at the rear of the belt. The mice were acclimated to the treadmill with two 15-min running sessions at 7° incline (10 m/min and 15 m/min belt speed) for 7 days, after which two exercise tests were performed on separate days: a performance test and an endurance test. The performance test began with a speed of 20 m/min, which was gradually increased by 10

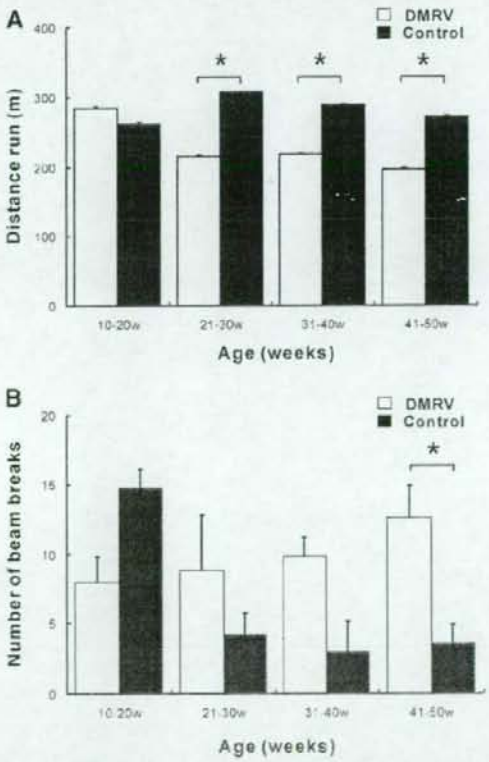

Fig. 2. Treadmill evaluation in mice. *A*: performance evaluation. Mice were given an increasing speed, and the distance that a mouse could run was measured at the point of exhaustion. At an early age, no difference was noted between control and DMRV mice. As mice aged, however, DMRV mice tended to cover a shorter distance in running compared with littermates. Data from male mice are shown. w, Week. *B*: endurance evaluation. A constant load was given to mice, and the number of beam breaks or rests, which is indirectly proportional to the ability of mice to endure the workload, was counted. Data from male mice are shown. Error bars represent SE. *$P < 0.05$. Values for male mice are shown; the same pattern is seen among female mice.

m/min every minute until the mouse was exhausted and could no longer run. Exhaustion was defined as the inability of the mouse to reengage the treadmill belt after 10 s of staying on the shock bars despite prodding. The time of exhaustion was used to calculate the distance the mouse covered during the exercise. The endurance exercise consisted of a 30-min treadmill run at 30 m/min with a 7° incline. During the test the total number of beam breaks was recorded, and this was inversely proportional to the ability of the mouse to sustain workload. A digital video camera was positioned above the treadmill to record each test; video recordings were used for analysis. Both tests were done three times, with a 3- to 4-day period of rest in between.

Contractile properties. Measurement of muscle contractile properties was performed according to previous protocols (6, 14), with some modifications. All materials used for in vitro measurement of force were acquired from Nihon Kohden (Tokyo, Japan). We analyzed the following muscles: gastrocnemius muscle, which is the preferentially involved muscle in terms of pathology; tibialis anterior (TA) muscle, which had no RVs even among aged DMRV mice; and quadriceps femoris (QF) muscle, because DMRV was initially known to be "quadriceps sparing." The mice were weighed and deeply anesthetized with pentobarbital sodium (40 mg/kg) intraperitoneally, with supplemental doses as necessary to maintain adequate anesthesia, which was judged by the absence of response to tactile stimuli.

The entire muscle was isolated, removed, and secured with a 4-0 silk suture at the distal muscle tendon and proximal bone of origin, after which the mice were killed by cervical dislocation. Subsequently, the muscle was mounted in a vertical chamber, connected to a force-displacement transducer (TB-652T for gastrocnemius and QF, TB-653T for TA), and positioned between a pair of platinum electrodes that delivered electrical stimulus. Throughout the analysis, the muscle was bathed in a physiological solution consisting of (in mM) 150 NaCl, 4 KCl, 2 $CaCl_2$, 1 $MgCl_2$, 5.6 glucose, 5 NaH_2PO_4 (pH 7.4), and 0.02 D-tubocurarine, maintained at a temperature of 20°C, and perfused continuously with a mixture of 95% O_2-5% CO_2 to facilitate acquisition of maximum level of force contraction as previously reported (6, 14). This supranormal oxygen level is nevertheless nonphysiological, because it has been shown to produce oxidative insult (10). Square wave pulses 0.2 ms in duration were generated by a stimulator (SEN-3301) and amplified (PP-106H), and subsequently muscle length was adjusted to the length (L_0) that resulted in maximal twitch force (P_t). With the muscle held at L_0 and the duration changed to 3 ms, the force developed during trains of stimulation pulses (10–200 Hz) was recorded.

Stimulation frequency was increased until the maximum absolute tetanic force (P_0) was achieved. For TA muscles 300-ms trains of pulses were used, while 600-ms trains were used for gastrocnemius. Data obtained were digitized and analyzed with a Leg-1000 polygraph system equipped with QP-111H software. Absolute force was normalized with the physiological cross-sectional area (CSA), which was computed as the product of the ratio of muscle weight and L_0 and the density for mammalian skeletal muscle, 1.066 mg/mm^3, to obtain specific force (P_t/CSA and P_0/CSA). After analysis of force generation, the muscles were removed from the chamber, blotted dry, and weighed.

Pathological and morphological analysis. Muscle tissues were processed for pathological analysis as previously reported (16). Serial cryosections were stained with hematoxylin and eosin, modified Gomori trichrome, and acid phosphatase according to standard procedures. Stained sections were visualized on a microscope (Olympus

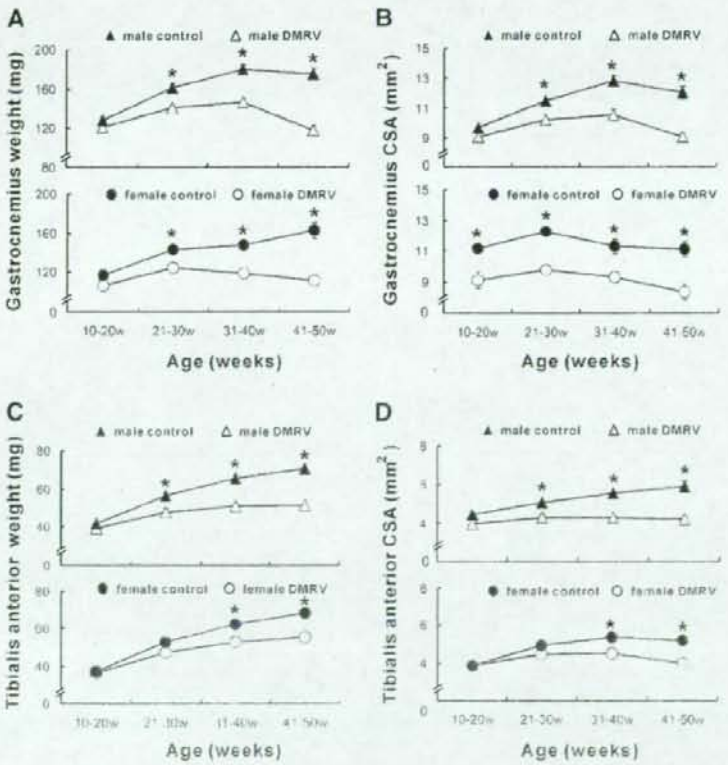

Fig. 3. Muscle mass and cross-sectional area (CSA). *A*: gastrocnemius muscle weight. *B*: gastrocnemius muscle CSA. *C*: tibialis anterior (TA) muscle weight. *D*: TA muscle CSA. In *A* and *C*, with the increasing body weight of control littermates, the masses of gastrocnemius (*A*) and TA (*C*) muscles show increase by 10–20% from 10 to 31 wk of age. From 40 to 50 wk of age, however, there is a very slight increase in the gastrocnemius muscles, while a slight decrease to no change was observed in the TA muscles. For the DMRV mice, muscles do not show any appreciable increases in weight from 21 wk of age and instead demonstrate a steadily decreasing muscle mass of at least 10–20% from 31 wk of age. In *B* and *D*, the CSA of both gastrocnemius (*B*) and TA (*D*) muscles in DMRV mice exhibit a delay in increase in CSA with age compared with control mice; as a result, the CSA is 10–15% less than that in control mice from 21 wk of age and decreases up to 40–50% by 50 wk. Values are expressed as means; error bars represent SE. $^*P < 0.05$.

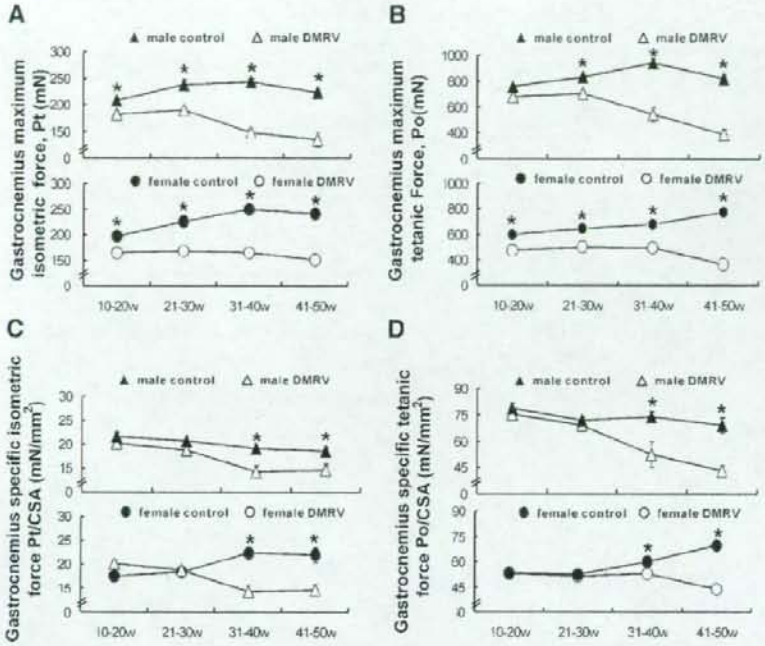

Fig. 4. Contractile properties of gastrocnemius muscle. *A*: peak isometric twitch (P_t). *B*: maximum tetanic force (P_0). *C*: P_t normalized by CSA, or specific P_t. *D*: P_0 normalized by CSA, or specific P_0. *A* and *B*: among littermates, P_t and P_0 follow a steady increase from 10 to 40 wk and gradual decrease thereafter, except in female mice. Among DMRV mice, a gradual decline is seen after 30 wk of age, with remarkable reduction after 40 wk of age; P_0 production seems to be more affected, because significant differences between DMRV and littermates are seen in all ages. *C* and *D*: force normalized by CSA shows similar pattern, except that remarkable differences are noted from 31 wk. Values are expressed as means. Error bars represent SE. $^*P < 0.05$.

BX51, Olympus, Melville, NY), and digitized images (DP70, Olympus) were acquired for pathological analysis. Congo red staining, visualized by fluorescence light, was likewise used to probe for intracellular inclusions (4).

Immunohistochemical analysis. For single-fiber CSA, sections were probed with β-dystroglycan (rabbit polyclonal antibody, a gift from Dr. Ejiro Ozawa, NIN, NCNP Tokyo, Japan) followed by appropriate secondary antibody. Images from six random areas of the muscles were captured at ×200 magnification. From these images, individual fiber diameter was measured from 600–800 fibers with J-image software (National Institutes of Health, **http://rsb.info.nih.gov/ij/**), taking note of the shortest diameter. Histological CSA was plotted and analyzed according to mouse group. Mouse monoclonal antibodies against myosin heavy chain (MHC) fast type and slow type (Novocastra, Newcastle upon Tyne, UK), BF-F3 (S. Schiaffino, ATCC) for MHC 2B, and SC-71 (S. Schiaffino, ATCC) for MHC 2A were used for muscle fiber type analysis.

Statistical analysis. All data are presented as means ± SE. For muscle mass and muscle contractile properties, repeated-measures (mixed model) ANOVA was used to determine the primary effects of age and genotype. Post hoc comparison by Bonferroni test was used to compare replicate rows. All statistical tests were considered to be significant when the error was <5% ($P < 0.05$). Our analysis showed that overall the effects of genotype on body weight, muscle weight, and contractile properties were not different for muscles of male and female mice (data not shown), but for clarity of presentation data from male and female mice are displayed separately and asterisks in Figs. 2–5 indicate only genotype differences, i.e., between DMRV and littermate mice. For single-fiber CSA, the data were not normally distributed. Consequently, cumulative frequency distributions of fiber sizes for each experimental group were determined and nonparametric statistical analyses were employed.

Table 1. *Contractile properties of DMRV muscles compared with control*

	10–20 wk	21–30 wk	31–40 wk	41–50 wk
Gastrocnemius, male				
Isometric	84.65	80.46	60.66	63.61
Specific isometric	91.88	90.55	74.10	86.62
Tetanic	89.36	85.26	57.66	51.25
Specific tetanic	96.70	96.17	70.66	69.48
P_t-to-P_0 ratio	97.35	94.06	107.72	125.96
Gastrocnemius, female				
Isometric	86.63	74.72	66.53	63.12
Specific isometric	108.15	94.14	80.42	89.07
Tetanic	78.38	77.79	73.04	44.95
Specific tetanic	98.13	97.75	88.10	61.62
P_t-to-P_0 ratio	107.19	95.88	90.88	133.18
Tibialis anterior, male				
Isometric	86.03	82.05	70.58	63.44
Specific isometric	96.82	97.09	92.51	89.66
Tetanic	82.86	75.81	63.11	56.91
Specific tetanic	93.18	90.12	82.02	80.28
P_t-to-P_0 ratio	103.69	108.04	110.96	109.76
Tibialis anterior, female				
Isometric	90.09	86.27	68.87	46.51
Specific isometric	89.72	96.13	81.95	60.70
Tetanic	88.18	89.52	74.19	50.88
Specific tetanic	87.87	99.47	88.33	66.42
P_t-to-P_0 ratio	100.87	97.74	93.87	96.29

DMRV, distal myopathy with rimmed vacuoles; P_t, isometric twitch force; P_0, tetanic force.

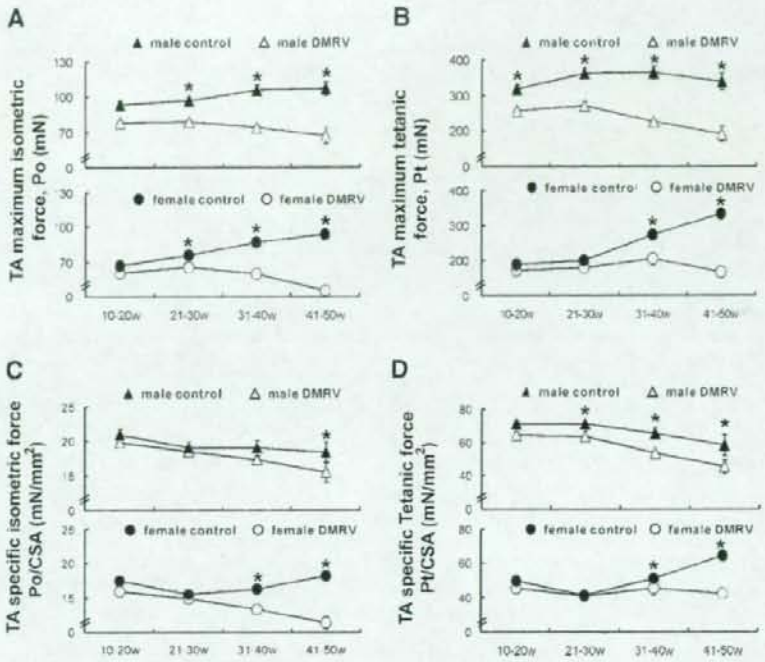

Fig. 5. Contractile properties of TA muscle. *A*: P_t. *B*: P_{to}. *C*: P_t normalized by CSA, or specific P_t. *D*: P_{to} normalized by CSA, or specific P_{to}. *A* and *B*: P_t and P_{to} in littermates are noted to increase steadily with age, except in P_{to} in male mice, in which there is a slight decrease after 40 wk of age. Among DMRV mice, there was a steady decrease in force production with age, and a significant difference became obvious from 21 wk of age. When normalized with CSA (*C* and *D*), however, remarkable differences in P_t/CSA between DMRV mice and littermates are only seen at 31 wk in female mice, while in specific P_{to} this difference is noted at 31 wk among male mice and at 41 wk among female mice. Error bars represent SE. $^*P < 0.05$.

RESULTS

Gross morphology of mice. The DMRV mice weighed less, and this difference in weight became more remarkable with age (Fig. 1). Body masses of both male and female control littermates increased 35–40% between 10 and 31 wk of age, with barely appreciable changes from 41 to 50 wk. In contrast, DMRV mice were at least 5–10% smaller at 10 wk of age and only showed small increases of body mass with age. Weight among these mice reached a plateau at around 30 wk of age, but decreased considerably from 41 wk.

DMRV mouse impaired motor performance and reduced endurance by treadmill analysis. When subjected to increasing workload, the DMRV mice performed worse than their littermates. The total distance they were able to run before total exhaustion was significantly less than that of control mice, and this was evident from the age of 21 wk in both males and females (Fig. 2*A*; data of female mice not shown). When given a consistent workload, the DMRV mice had greater beam breaks, reflecting less ability for endurance, although significant differences were only noted at 41–50 wk (Fig. 2*B*) because of large error bars.

Decreased muscle weight and CSA contribute to weight loss in DMRV mice. Both the gastrocnemius and TA muscles of DMRV mice weighed less compared with control mice (Fig. 3, *A* and *C*). More remarkable and more significant statistical differences were noted in the older age groups. In addition, the muscles did not show any appreciable increases in weight from 21 wk of age and instead demonstrated a steadily decreasing muscle mass of at least 10–20% from 31 wk of age, with more remarkable decrease in muscle mass of gastrocnemius from 41 wk of age.

Compatible with the pattern of muscle mass with age, the whole muscle CSA of both muscles in DMRV mice rather exhibited a delay in increase in CSA with age compared with control mice (Fig. 3, *B* and *D*); as a result, the CSA is 10–15% less than control mice from 21 wk of age and decreases by 40–50% more with age than that of control mice by 50 wk.

The quadriceps muscles of the DMRV mice were also affected, but at a much later age. From 31 wk of age, the QF muscles were lighter and had lower CSA compared with control (Supplemental Fig. S1).[1]

Muscle contractile properties. In DMRV gastrocnemius muscles, P_t and P_{to} showed gradual decrements with age (Fig. 4, *A* and *B*) compared with control: 90% by 10 wk, 80% by 21 wk, 70% by 31 wk, and 50% by 41 wk. Of note, the P_{to} values were markedly reduced after 41 wk of age (Fig. 4*B*); thus when the twitch-tetanic ratio is computed, it is significantly higher in both male and female DMRV mice compared with control mice (Table 1). Specific P_t and P_{to} values showed similar temporal pattern of force reduction in DMRV mice (Fig. 4, *C* and *D*), except that significant differences between DMRV and control mice were only seen from the age of 31 wk.

In DMRV TA muscles, P_t showed a different pattern with age, in contrast to control (Fig. 5, *A* and *B*), slightly increasing from 10 to 20 wk and then gradually decreasing from 21 wk

[1] The online version of this article contains supplemental material.

onward. Furthermore, P_t was notably lower in all age groups, despite the absence of any noted abnormality in pathology. P_0 values in these model mice were likewise lower than in control mice in all age groups, similar to the gastrocnemius, but with statistical significance at 21 wk of age in male mice and at 31 wk of age in female mice. Similar to the gastrocnemius muscles, the specific P_t values of TA muscles of DMRV mice were nearly normal during early age; remarkable reduction was only seen from 31 wk (Fig. 5, *C* and *D*). Table 1 further summarizes the contractile properties of the gastrocnemius and TA muscles of the DMRV mice compared with littermates. Overall, ~10–50% deficit in generation of force is observed in these muscles.

The QF muscles of the DMRV mice showed reduction of both P_0 and P_t from 31 wk of age, but no differences with respect to control mice were seen when these values were normalized with CSA (Supplemental Fig. S2).

Atrophic changes are noted before development of pathological hallmarks in DMRV muscle. From 10 to 20 wk of age the muscles from the DMRV mice appear morphologically unremarkable on light microscopy, except for minimal variation in fiber size in the gastrocnemius (Fig. 6*A*), TA (Fig. 7*A*), and QF (Supplemental Fig. S3*A*) muscles. For both gastrocnemius and TA muscles, the number of small-sized fibers increases from 21 to 30 wk of age, contributing to the variation in fiber size. From 31 to 40 wk of age, scattered

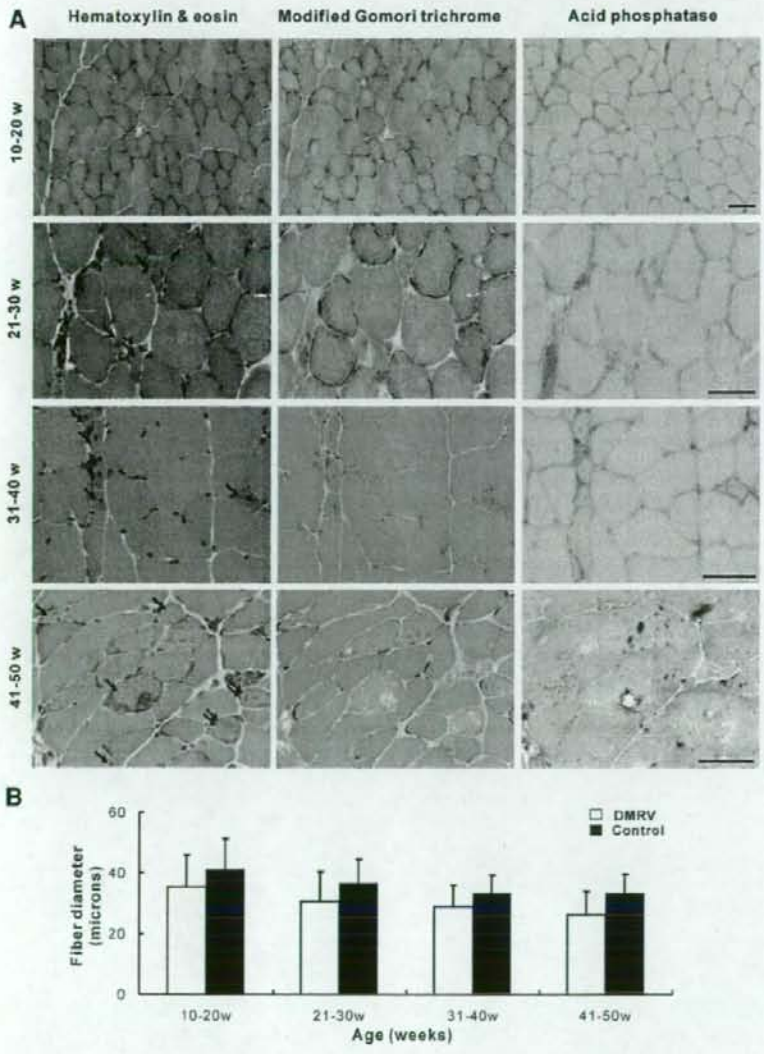

Fig. 6. Gastrocnemius muscle: pathological findings and single-fiber CSA. *A*: hematoxylin and eosin (H&E) and modified Gomori trichrome (mGT) sections show only mild variation in fiber size in gastrocnemius muscle of DMRV mice at 10–20 wk, almost indistinguishable from control. No endomysial fibrosis or inflammation is seen. Small atrophic fibers are seen randomly (black arrows) and are observed by 21–30 wk, and the number of such fibers tends to increase by 31–40 wk, making the variation in fiber size more remarkable. By 41–50 wk, rimmed vacuoles (RVs) (red arrows) are noted to be scattered in the muscle. These RVs are more highlighted in mGT and are stained in acid phosphatase, indicating upregulation of the lysosomal system. Double arrows show intracellular inclusions. Bars, 50 μm. *B*: single-fiber CSA shows the variation in fiber size, which is more remarkable in DMRV mice as they age. Note that myofibers of DMRV mice are generally smaller at all ages, implying gradual decrease in the caliber of fibers. Values are expressed as means; error bars represent SD.

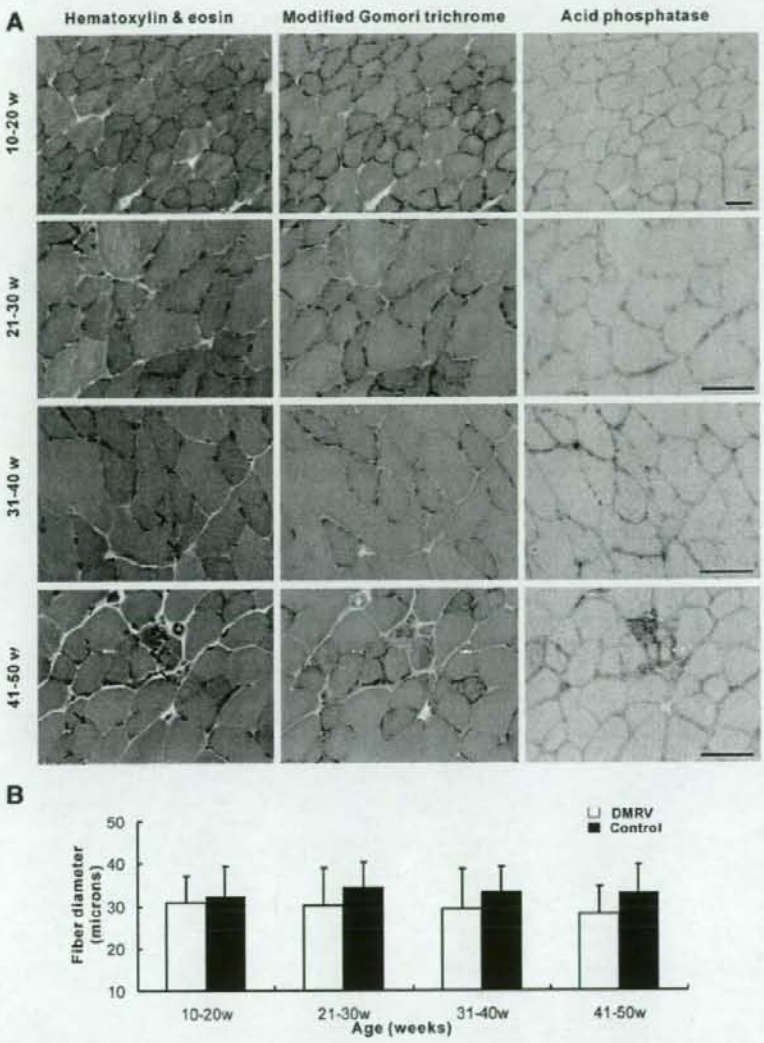

Fig. 7. TA muscle: pathological findings and single-fiber CSA. *A*: H&E and mGT sections from TA muscles show only subtle changes, including mild variation in fiber size. No endomysial fibrosis or inflammation is seen. Small atrophic fibers (black arrows) are observed by 21–30 wk, and the number of such fibers increases by 31–40 wk, making the variation in fiber size more remarkable. In contrast to the gastrocnemius, no RVs are noted even at the older stage. Bars, 50 μm. *B*: single-fiber CSA shows the variation in fiber size, which is more remarkable in DMRV mice as they age. The means of fiber CSA are generally lower in DMRV mice compared with control. Values are expressed as means; error bars represent SD.

small angular fibers are observed. At this age, at least in the gastrocnemius, there are few intracellular inclusions, which are Congo red positive (data not shown) and immunoreactive to various antibodies to amyloid β as we demonstrated previously (16). RVs are noted from 42 wk and in older mice in the gastrocnemius muscles, while none is seen in the TA. Interestingly, the same changes were seen in the QF (Supplemental Fig. S3*A*), although the onset of changes notably occurred at a later age; the presence of small atrophic fibers was noted from 30 wk; few Congo red-positive inclusions were seen after 40 wk; and some RVs were visible after 50 wk.

By measuring the diameter of fibers in both gastrocnemius and TA muscles, we found that fiber size in DMRV mice is almost normal and comparable to littermates from 10 to 20 wk of age. After 20 wk of age, however, remarkable variations in fiber size were seen in both gastrocnemius and TA muscles (Figs. 6*B* and 7*B*), and the frequency of smaller-sized fibers increased with age, shifting the histogram to the left (Supplemental Fig. S4) and providing further evidence of atrophy. Similarly, the fibers of QF muscles also appear smaller, but the variation is much more evident after 40 wk of age (Supplemental Fig. S5).

Muscle atrophy affects both fiber type I and type II. In terms of fiber type effect, we did not find fiber type predominance in DMRV muscles (data not shown). At least in gastrocnemius (Fig. 8*A*, *top*), TA (Fig. 8*A*, *bottom*), and QF (Supplemental Fig. S4) muscle, we noted reduction in individual fiber CSA in

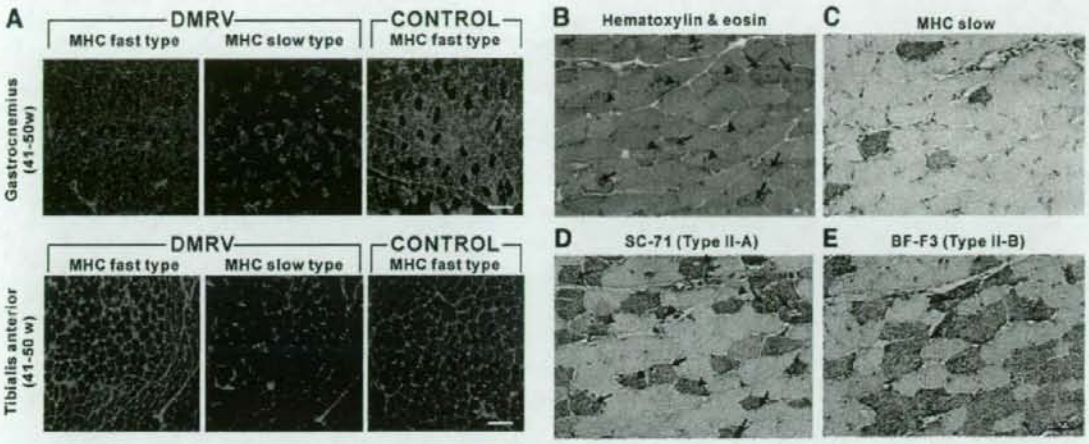

Fig. 8. Muscle atrophy involves both type I and type II fibers. *A*: representative sections from gastrocnemius (*top*) and TA (*bottom*) muscles stained with myosin heavy chain (MHC) fast fiber type and MHC slow fiber type. Compared with control, both type I and type II fibers in DMRV muscles are smaller. *B*: muscle cryosections from the gastrocnemius muscles (44-wk-old female DMRV mouse) were stained with H&E showing myofibers with RVs (arrows) and inclusion bodies (arrowheads), in addition to marked variation in fiber size. *C*: MHC slow type for type I (slow) fibers. *D*: MHC fast type for type II (fast) fibers. *E*: BF-F3, which recognizes type 2B (fast glycolytic) fibers. Note that fibers with RVs and inclusions are virtually type IIA (fast oxidative) fibers, as shown by positive staining for SC-71 (*D*). Bars, 50 μm.

both fast and slow fibers (quantitative data not shown). Interestingly, almost all fibers that had either RVs or intracellular depositions were type II fibers (Fig. 8, *B* and *C*) and were fast oxidative type (Fig. 8, *D* and *E*).

DISCUSSION

Through the analysis of structure and function of the muscles of DMRV mice, we found that skeletal muscles exhibit atrophy and that this phenomenon is well-correlated with reduction in force generation and, consequently, development of muscle weakness. More importantly, the onset of muscle atrophy predated the pathological hallmarks of DMRV, which include intracellular inclusion body and RV formation, and may be regarded to have a greater contribution to the development of muscle symptoms than RV formation per se.

The overall muscle fiber size is determined by the balance between synthesis and degradation of intracellular components. Muscle atrophy occurs when the protein degradation rate is higher than the synthesis rate and is noted in several situations like disuse, fasting, aging, and a number of disease states. Because of the variety of conditions in which muscle atrophy is evident, different signaling pathways and molecular triggers are thought to determine the activation of target systems responsible for decreased protein synthesis or increased proteolysis.

Three proteolytic systems that have been implicated in muscle wasting are the ubiquitin-proteasome (UPS) (5, 27), lysosomal (13, 30), and calpain (7) systems. The activity of UPS is markedly increased in atrophying muscles, mainly because of the transcriptional activation of two muscle-specific ubiquitin ligases, namely, atrogin-1 and Murf-1, among other genes. The expression of these ubiquitin ligases is mainly activated by two major signaling pathways, including FoxO and NF-κB. Recently, FoxO3 was demonstrated to control both UPS and lysosomal pathways (17); thus it will be very interesting to see whether the same mechanism is involved in DMRV, because activation of both the UPS and lysosomal systems have been demonstrated in this myopathy. Such systems, however, are thought to be stimulated as a response to accumulation of various proteins in the myofibers (29). This, however, could not entirely explain the phenomenon of muscle atrophy in the young DMRV mice, in which there are virtually no abnormal intracellular protein accumulations that could trigger these proteolytic systems. Thus it is more likely that it could involve the activation of certain upstream molecular signals that may initiate myofibrillar proteolysis; this notion is worth exploring to get other clues for understanding how muscles atrophy in DMRV.

The relationship of fiber type involvement and pathological changes in DMRV has not been fully clarified, although it has been suggested that type II fibers are predominantly affected (25). The preferential involvement of type II fibers in the gastrocnemius muscles of DMRV mice, in terms of RV formation and intracellular protein deposition, is not clear at the moment. The predominant involvement of type II muscle fibers in other murine models of muscular dystrophy and myopathies (24) has been presumed to be due to the increased susceptibility of these muscles to eccentric contraction-induced damage (8, 33). In the DMRV mice, this is intriguing since the mechanism underlying the disease is remarkably different from these other murine models. However, in a transgenic mouse overexpressing β-amyloid precursor protein (β-APP) intracellular amyloid deposition has been noted predominantly in type II fibers (28). This could suggest that the involvement of fast-type fibers may be secondary to poor endocytic trafficking and vesicular fusion, characteristics that have been attributed to fast-type fibers. Moreover, in a mouse overexpressing β-APP in type II fibers, an increase in resting calcium and relative membrane depolarization in muscle fibers have been observed and are thought to represent a mechanism relating β-APP

mismetabolism to altered calcium homeostasis and clinical weakness (19). Because intracellular amyloid depositions are seen in muscles of DMRV mice, this topic may be of interest for future investigations.

By analyzing physiological properties of the muscle in DMRV mice, we have seen that as the mice age the difference in force production becomes more remarkable. At least in the gastrocnemius muscle, the reduction of force can be attributed to muscle atrophy during the earlier ages. From 31 to 40 wk of age, the presence of intracellular deposits may interfere with the function of myofibrils. From 41 to 50 wk, the remarkable reduction in force generation can be attributed to RV formation and muscle degeneration, which subsequently lead to myofibrillar disorganization and interfere with sarcomeric contraction.

It is of particular interest, however, that isometric twitches are particularly affected at 31–40 wk of age, the age at which inclusion bodies start to appear, while tetanic forces are predominantly affected at the age of RV formation. This may imply that other signaling pathways in skeletal muscle contraction can be affected as well. The fact that the P_t-to-P_0 ratio is increased from 41 wk would additionally suggest that the contribution of RV formation to weakness is greater than the influence of the presence of intracellular inclusions. The same deduction, however, cannot be applied to the DMRV TA muscles, in which both P_t and P_0 values follow a gradual reduction in an age-related manner, but where P_0 and P_0/CSA values are markedly reduced at 41–50 wk. It is tempting to speculate that the P_t-to-P_0 ratio is actually maintained because of the absence of structural pathological changes in these muscles, but this would need further studies.

The analysis of the physiological properties of muscles in DMRV mice allowed us to demonstrate that atrophy is indeed evident in the muscles of these DMRV mice, and this seems to play a major role in the reduced generation of muscle force, especially in the early ages before the appearance of RVs and/or inclusion bodies. Furthermore, our data suggest that RV formation is most likely a downstream event in the pathogenesis of DMRV. But because the most constant finding that we have seen in all age groups is hyposialylation (16) long before the development of any muscle phenotype, further studies to elucidate how decreased sialylation triggers the complicated pathways leading to atrophy may give further clues on disease pathomechanism.

GRANTS

This study was supported partly by the "Research on Psychiatric and Neurological Diseases and Mental Health" from the Japanese Health Sciences Foundation, partly by the Program for Promotion of Fundamental Studies in Health Sciences of the National Institute of Biomedical Innovation (NIBIO), partly by the "Research Grant (17A-10, 19A-7) for Nervous and Mental Disorders" from the Ministry of Health Labour and Welfare, partly by the Kato Memorial Trust for Nambyo Research, and partly by the Neuromuscular Disease Foundation.

ACKNOWLEDGMENTS

The authors acknowledge the valuable assistance offered by Ryuta Hoshi, Dr. Kazunari Momma, and Yu Matsuda in the motor performance evaluation of mice.

REFERENCES

1. **Akanas V, Engel WK.** Proposed pathogenic cascade of inclusion-body myositis: importance of amyloid-beta, misfolded proteins, predisposing genes, and aging. *Curr Opin Rheumatol* 15: 734–744, 2003.
2. **Amsili S, Shlomai Z, Levitzki R, Krause S, Lochmuller H, Ben-Bassat H, Mitrani-Rosenbaum S.** Characterization of hereditary inclusion body myopathy myoblasts: possible primary impairment of apoptotic events. *Cell Death Differ* 14: 1916–1924, 2007.
3. **Argov Z, Yarom R.** "Rimmed vacuole myopathy" sparing the quadriceps. A unique disorder in Iranian Jews. *J Neurol Sci* 64: 33–43, 1984.
4. **Askanas V, Engel WK, Alvarez RB.** Enhanced detection of Congo-red-positive amyloid deposits in muscle fibers of inclusion body myositis and brain of Alzheimer's disease using fluorescence technique. *Neurology* 43: 1265–1267, 1993.
5. **Clarke BA, Drujan D, Willis MS, Murphy LO, Corpina RA, Burova E, Rakhilin SV, Stitt TN, Patterson C, Latres E, Glass DJ.** The E3 ligase MuRF1 degrades myosin heavy chain protein in dexamethasone-treated skeletal muscle. *Cell Metab* 6: 376–385, 2007.
6. **Consolino C, Duclos F, Lee J, Williamson RA, Campbell KP, Brooks S.** Muscles of mice deficient in α-sarcoglycan maintain large masses and near control force values throughout the life span. *Physiol Genomics* 22: 244–256, 2005.
7. **Costelli P, Reffo P, Penna F, Autelli R, Bonelli G, Baccino FM.** Ca^{2+}-dependent proteolysis in muscle wasting. *Int J Biochem Cell Biol* 37: 2134–2146, 2005.
8. **D'Antona G, Brocca L, Pansarasa O, Rinaldi C, Tupler R, Bottinelli R.** Structural and functional alterations of muscle fibres in the novel mouse model of facioscapulohumeral muscular dystrophy. *J Physiol* 584.3: 997–1009, 2007.
9. **Eisenberg I, Avidan N, Potikha T, Hochner H, Chen M, Olender T, Barash M, Shemesh M, Sadeh M, Grabov-Nardini G, Shmilevich I, Friedmann A, Karpati G, Bradley WG, Baumbach L, Lancet D, Asher EB, Beckmann JS, Argov Z, Mitrani-Rosenbaum S.** The UDP-*N*-acetylglucosamine 2-epimerase/*N*-acetylmannosamine kinase gene is mutated in recessive hereditary inclusion body myopathy. *Nat Genet* 29: 83–87, 2001.
10. **Eu JP, Hare JM, Hess DT, Skaf M, Sun J, Cardenas-Navina I, Sun Q, Dewhirst M, Meissner G, Stamler JS.** Concerted regulation of skeletal muscle contractility by oxygen tension and endogenous nitric oxide. *Proc Natl Acad Sci USA* 100: 15229–15234, 2003.
11. **Gabellini D, D'Antona G, Moggio M, Zecca C, Adami R, Angeletti B, Pellegrino MA, Botinelli R, Green MR, Tupler R.** Facioscapulohumeral muscular dystrophy in mice overexpressing FRG1. *Nature* 439: 973–977, 2006.
12. **Kayashima T, Matsuo H, Satoh A, Ohta T, Yoshiura K, Matsumoto N, Nakane Y, Niikawa N, Kishino T.** Nonaka myopathy is caused by mutations in the UDP-*N*-acetylglucosamine-2-epimerase/*N*-acetylmannosamine kinase gene (*GNE*). *J Hum Genet* 47: 77–79, 2002.
13. **Lum JJ, DeBerardinis RJ, Thompson CB.** Autophagy in metazoans: cell survival in the land of plenty. *Nat Rev Mol Cell Biol* 6: 439–448.
14. **Lynch GS, Hinkle RT, Chamberlain JS, Brooks SV, Faulkner J.** Force and power output of fast and slow skeletal muscles from mdx mice 6–28 months old. *J Physiol* 535.2: 591–600, 2001.
15. **Malicdan MC, Noguchi S, Nishino I.** Autophagy in a mouse model of distal myopathy with rimmed vacuoles or hereditary inclusion body myopathy. *Autophagy* 3: 396–398, 2007.
16. **Malicdan MC, Noguchi S, Nonaka I, Hayashi YK, Nishino I.** A *Gne* knockout mouse expressing human *GNE* D176V mutation develops features similar to distal myopathy with rimmed vacuoles or hereditary inclusion body myopathy. *Hum Mol Genet* 16: 2669–2682, 2007.
17. **Mammucari C, Milan G, Romanello V, Masiero E, Rudolf R, Del Piccolo P, Burden SJ, Di Lisi R, Sandri C, Zhao J, Goldberg A, Schiaffino S, Sandri M.** FoxO3 controls autophagy in skeletal muscle in vivo. *Cell Metab* 6: 458–471, 2007.
18. **Mirabella M, Alvarez RB, Bilak M, Engel WK, Askanas V.** Difference in expression of phosphorylated tau epitopes between sporadic and hereditary inclusion-body myopathies. *J Neuropathol Exp Neurol* 55: 774–786, 1996.
19. **Moussa CE, Fu Q, Kumar P, Shtifman A, Lopez JR, Allen PD, LaFerla F, Weinberg D, Magrane J, Aprahamian T, Walsh K, Rosen KM, Querfurth HW.** Transgenic expression of beta-APP in fast-to-itch skeletal muscle leads to calcium dyshomeostasis and IBM-like pathology. *FASEB J* 12: 2165–2167, 2006.

20. **Nishino I, Malicdan MC, Murayama K, Nonaka I, Hayashi YK, Noguchi S.** Molecular pathomechanism of distal myopathy with rimmed vacuoles. *Acta Myol* 24: 80–83, 2005.
21. **Nishino I, Noguchi S, Murayama K, Driss A, Sugie K, Oya Y, Nagata T, Chida K, Takahashi T, Takusa Y, Ohi T, Nishimiya J, Sunohara N, Ciafaloni E, Kawai M, Aoki M, Nonaka I.** Distal myopathy with rimmed vacuoles is allelic to hereditary inclusion body myopathy. *Neurology* 59: 1689–1693, 2002.
22. **Noguchi S, Keira Y, Murayama K, Ogawa M, Fujita M, Kawahara G, Oya Y, Imazawa M, Goto Y, Hayashi YK, Nonaka I, Nishino I.** Reduction of UDP-*N*-acetylglucosamine 2-epimerase/*N*-acetylmannosamine kinase activity and sialylation in distal myopathy with rimmed vacuoles. *J Biol Chem* 279: 11402–11407, 2004.
23. **Nonaka I, Noguchi S, Nishino I.** Distal myopathy with rimmed vacuoles and hereditary inclusion body myopathy. *Curr Neurol Neurosci Rep* 5: 61–65, 2005.
24. **North KN, Laing NG, Wallgren-Pettersson C.** Nemaline myopathy: current concepts. The ENMC International Consortium on Nemaline Myopathy. *J Med Genet* 34: 705–713, 1997.
25. **Ricci E, Broccolini A, Gidaro T, Morosetti R, Gliubizzi C, Frusciante R, Di Lella GM, Tonali PA, Mirabella M.** NCAM is hyposialylated in hereditary inclusion body myopathy due to GNE mutations. *Neurology* 66: 755–758, 2006.
26. **Richard I, Roudaut C, Marchand S, Baghdiguian S, Herasse M, Stockholm D, Ono Y, Suel L, Bourg N, Sorimachi H, Lefranc G, Fardeu M, Sebille A, Beckmann JS.** Loss of calpain 3 proteolytic activity leads to muscular dystrophy and to apoptosis-associated IκBα/nuclear factor κB pathway perturbation in mice. *J Cell Biol* 151: 1583–1590, 2000.
27. **Solomon V, Baracos V, Sarraf P, Goldber AL.** Rates of ubiquitin conjugation increase when muscle atrophy, largely through activation of N-end rule pathway. *Proc Natl Acad Sci USA* 95: 12602–12607, 1998.
28. **Sugarman MC, Kitazawa M, Baker M, Caiozzo VJ, Querfurth HW, LaFerla FM.** Pathogenic accumulation of APP in fast twitch muscle of IBM patients and a transgenic model. *Neurobiol Aging* 27: 423–432, 2006.
29. **Tsuruta Y, Furuta A, Furuta K, Yamada T, Kira J, Iwaki T.** Expression of the lysosome-associated membrane proteins in myopathies with rimmed vacuoles. *Acta Neuropathol* 101: 579–584, 2001.
30. **Voisin L, Breuillé D, Combaret L, Pouyet C, Taillandier D, Aurousseau E, Obled C, Attaix D.** Muscle wasting in a rat model of long-lasting sepsis results from the activation of lysosomal, Ca^{2+}-activated, and ubiquitin-proteasome proteolytic pathways. *J Clin Invest* 97: 1610–1617, 1996.
31. **Wang Z, Sun Z, Li AV, Yarema KJ.** Roles for GNE outside of sialic acid biosynthesis: modulation of sialyltransferase and BiP expression, GM3 and GD3 biosynthesis, proliferation and apoptosis, and ERK1/2 phosphorylation. *J Biol Chem* 281: 27016–27028, 2006.
32. **Yan C, Ikezoe K, Nonaka I.** Apoptotic muscle fiber degeneration in distal myopathy with rimmed vacuoles. *Acta Neuropathol* 101: 9–16, 2001.
33. **Yeung EW, Head SI, Allen DG.** Gadolinium reduces short-term stretch-induced muscle damage in isolated mdx mouse muscle fibers. *J Physiol* 552: 449–458, 2003.

SHORT REPORT

ABSTRACT: In Ullrich congenital muscular dystrophy, due to heterozygous mutations in *COL6* genes, collagen VI is preserved in the interstitium but lost in the sarcolemma. We found that the binding ability of mutated collagen VI to extracellular matrix was markedly reduced compared to control. This indicates that heterozygous mutations in *COL6* genes diminish the anchorage of collagen VI microfibrils to the extracellular matrix surrounding myocytes. This is the cause for sarcolemma-specific collagen VI deficiency.

Muscle Nerve **38:** 1192–1195, 2008

DIMINISHED BINDING OF MUTATED COLLAGEN VI TO THE EXTRACELLULAR MATRIX SURROUNDING MYOCYTES

GENRI KAWAHARA, PhD,[1] MEGUMU OGAWA, MS,[1] MARI OKADA, MD,[1,3] MAY CHRISTINE V. MALICDAN, MD,[1] YU-ICHI GOTO MD, PHD,[2] YUKIKO K. HAYASHI, MD, PhD,[1] SATORU NOGUCHI, PhD,[1] and ICHIZO NISHINO, MD, PhD[1]

[1] Department of Neuromuscular Research, National Institute of Neuroscience, National Center of Neurology and Psychiatry (NCNP), 4-1-1 Ogawahigashi-cho, Kodaira, Tokyo, Japan.
[2] Department of Mental Retardation and Birth Defect Research, National Institute of Neuroscience, National Center of Neurology and Psychiatry (NCNP), Tokyo, Japan.
[3] Second Department of Pediatrics, Toho University School of Medicine, Tokyo, Japan.

Accepted 27 February 2008

Ullrich congenital muscular dystrophy (UCMD) is an inherited muscular disorder characterized clinically by muscle weakness, distal joint hyperlaxities, and proximal joint contractures.[1,4] UCMD patients show deficiency of collagen VI. We have previously demonstrated two modes of collagen VI deficiency based on immunohistochemistry: complete deficiency (CD)[4,6] and sarcolemma-specific collagen VI deficiency (SSCD). In SSCD, collagen VI is present in the interstitium but is barely detectable in the sarcolemma.[7]

Collagen VI is an extracellular matrix (ECM) component consisting of three chains, α1, 2, and 3, which are encoded by *COL6A1*, *COL6A2*, and *COL6A3*, respectively.[2,3,15] Recent reports showed that UCMD patients with SSCD have heterozygous missense mutations in *COL6A1*, including p.G284R, which lead to glycine substitution in the Gly-*X*-*Y* amino acid repeat in the triple helical domain (THD).[1,5,10] Collagen VI microfibrils harboring p.G284R in *COL6A1* cause reduced cell adhesion of fibroblasts.[8,11]

In this article we report that the binding of mutated collagen VI to ECM surrounding myocytes is reduced, and this plays an important role in the pathomechanism of SSCD.

MATERIALS AND METHODS

Clinical Materials. All subjects enrolled in this study were acquired with informed consent. We studied six Japanese patients who were diagnosed as having UCMD based on typical clinical features, i.e., muscle weakness, hyperextensibility of distal joints, and contractures of proximal joints.[11]

Skin fibroblasts in this study were from six patients with SSCD, one patient with CD, and one from a normal control. In the six patients *COL6* mutations had been identified by sequence analysis; heterozygous mutation in THD. Patient 1: c.850G>A (p.G284R) in *COL6A1*; Patient 2: c.868G>A (p.G290R) in *COL6A1*; Patient 3: c.958_966del9 (p.G320_K322del) of *COL6A1*; Patient 4: c.1056+1 G>A (p.G335_D352) in

Abbreviations: CD, complete deficiency; DMEM, Dulbecco's modified Eagle medium; ECM, extracellular matrix; SSCD, sarcolemma-specific collagen VI deficiency; THD, triple helical domain; UCMD, Ullrich congenital muscular dystrophy

Key words: collagen VI; extracellular matrix; myocyte; triple helical domain; Ullrich congenital muscular dystrophy

Correspondence to: I. Nishino; e-mail: nishino@ncnp.go.jp

Published online 18 July 2008 in Wiley InterScience (www.interscience.wiley.com). DOI 10.1002/mus.21030